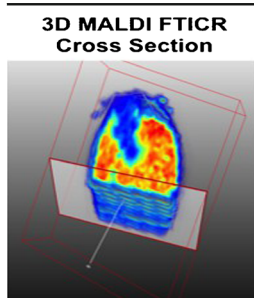CrossMark

RESEARCH ARTICLE

Feasibility Assessment of a MALDI FTICR Imaging Approach for the 3D Reconstruction of a Mouse Lung

E. Ellen Jones, Cristine Quiason, Stephanie Dale, Sheerin K. Shahidi-Latham

Department of Drug Metabolism and Pharmacokinetics, Genentech, Inc., 1 DNA Way MS 41-2a, South San Francisco, CA 94080, USA

3D MALDI FTICR Cross Section

Abstract. Matrix assisted laser desorption ionization imaging mass spectrometry (MALDI IMS) has proven to be a quick, robust, and label-free tool to produce two-dimensional (2D) ion-density maps representing the distribution of a variety of analytes across a tissue section of interest. In addition, three-dimensional (3D) imaging mass spectrometry workflows have been developed that are capable of visualizing these same analytes throughout an entire volume of a tissue rather than a single cross-section. Until recently, the use of Fourier transform ion cyclotron resonance (FTICR) mass spectrometers for 3D volume reconstruction has been impractical due to software limitations, such as inadequate capacity to manipulate the extremely large data files produced during an imaging experiment. Fortunately with recent software and hardware advancements, 3D reconstruction from MALDI FTICR IMS datasets is now feasible. Here we describe the first proof of principle study for a 3D volume reconstruction of an entire mouse lung using data collected on a FTICR mass spectrometer. Each lung tissue section was analyzed with high mass resolution and mass accuracy, and considered as an independent dataset. Each subsequent lung section image, or lung dataset, was then co-registered to its adjacent section to reconstruct a 3D volume. Volumes representing various endogenous lipid species were constructed, including sphingolipids and phosphatidylcholines (PC), and species confirmation was performed with on-tissue collision induced dissociation (CID).

Keywords: MALDI, Imaging mass spectrometry, Lipid, 3D, Three-dimensional, Volume, FTICR, IMS, Lung, Matrix-assisted laser desorption, High-resolution

Introduction

Matrix assisted laser desorption ionization imaging mass spectrometry (MALDI IMS) is a robust, label-free technique in which an analyte of interest can be visualized across a tissue section in relation to the tissue's histopathology [1–3]. From its inception in the late 1990s until today, there have been many successful imaging studies analyzing proteins, peptides, lipids, small molecule drugs, and n-linked glycans from tissues of interest [4–10]. Although the earliest imaging efforts focused primarily on the detection of protein and peptide distributions in human and animal tissues, subsequent studies have successfully applied MALDI IMS to a variety of sample types and disciplines, while also producing novel methods for sample preparation and matrix application [11–15]. Recent incorporation of high-resolution mass spectrometers such as a Fourier transform ion cyclotron resonance mass spectrometer (FTICR MS) within imaging workflows has further advanced the field of IMS, making previously hard to distinguish small molecule metabolites attainable with high resolving power and mass accuracy [16, 17].

The on-going success of MALDI IMS studies demonstrate the utility of the workflow to visualize distributions of analytes across a tissue section of interest; however, conventional IMS workflows still remain limited to a single cross-section of tissue. Considering that biological systems are not confined to 2D, and in the context of tissues such as tumors, which can have a heterogeneous population of cells influencing the disease pathology, interrogating a single cross-section may

---

E. Ellen Jones and Sheerin K. Shahidi-Latham have contributed equally to this work.

Correspondence to: Shaerin K. Shahidi–Latham; *e-mail:* sheerink@gene.com

misrepresent important features occurring throughout the entire tissue volume [18]. Although it is possible to systematically acquire sequential data from serial sections of an entire organ, a comprehensive assessment would still require independent evaluations of each 2D slice, ultimately limiting the contextual value of potentially unique observations in the z-plane. Alternatively, accurately stacking and co-registering these 2D datasets in a 3D imaging approach provides a unique opportunity to visualize an organ volume, and further to preserve the contextual assessments of analyte distributions in the z-plane.

Currently, there are several 3D imaging modalities in use, including magnetic resonance imaging (MRI), positron emission technology (PET), and single-photon emission computed tomography (SPECT) [19–22]. While these in vivo technologies are effective at interrogating organ anatomy, they are limited in specificity unless a prelabeled analyte is administered and even then sensitivity is often lacking. Further, spatial resolutions of these techniques can also be relatively poor. In contrast, MALDI IMS can provide a highly multiplexed, label-free ex vivo approach to interrogate tissues with high specificity, sensitivity, and spatial resolution, making it a suitable and complementary 3D imaging modality.

Accordingly, 3D MALDI IMS studies have gained prominence, and their applications span various tissues, from cells, excised organs, to whole mouse pups, and demonstrate the ability to render volumes of vast analyte classes, including lipids and proteins [23–28]. Moreover, advancements in computer hardware as well as user-friendly software suites have been key drivers in the expanded popularity of 3D IMS datasets [29–31]. Work still remains for the development of software packages that allow for the integration of 3D MALDI IMS datasets with its complementary in vivo 3D imaging modalities; nevertheless, the concept has been successfully demonstrated with MRI using MATLAB (matrix laboratory) [24, 32]. Despite these advancements, 3D MALDI IMS datasets have been limited to low resolution mass spectrometers such as a MALDI Time-of-Flight MS. The absence of 3D MALDI IMS datasets from high mass resolution instruments, such as an FTICR MS, can be attributed to the massive data file sizes inherently produced by such instrumentation [33]. With the auspicious release of vendor-updated data acquisition software allowing for on-the-fly data reduction as well as third-party post-processing software tools capable of further compressing and managing the massive data loads, the opportunity to explore the feasibility of 3D FTICR IMS workflows is now possible. This paper represents the first successful 3D reconstruction of MALDI IMS data acquired on an FTICR mass spectrometer and its application to interrogating lipid distributions across a mouse lung volume.

Materials and Methods

2, 5-Dihydroxybenzoic acid (DHB) matrix and trifluoroacetic acid (TFA) were purchased from Sigma Aldrich (St. Louis, MO, USA). Methanol was purchased from EMD Millipore Corporation (Billerica, MA, USA), and indium tin oxide (ITO) slides were purchased from Bruker Daltonics (Billerica, MA, USA).

Tissue Preparation and FTICR MALDI-IMS Analysis

Lungs were collected from male Balb/c mice perfused with PBS and inflated with 1% CMC and snap frozen. The whole of lung was sectioned at 12-um thickness and sections for analysis were collected every 120-μm on a cryomicrotome (CM3050S; Leica, Buffalo Grove, IL, USA). A total of 40 sections were collected, representing the entire lung volume. Tissue sections were thaw mounted onto indium tin oxide-coated glass slides, and an optical image was obtained on a flatbed scanner prior to matrix deposition. Tissue slides were then spray-coated with 40 mg/mL 2, 5-dihydroxybenzoic acid (DHB) matrix in 70% methanol using an HTX TM-sprayer (HTX Technologies, Chapel Hill, NC, USA). Matrix was applied in eight passes with a flow rate of 0.2 mL/min. A nozzle temperature of 75 °C, dry time of 0.5 min in between passes, 3 mm line spacing, and a spray velocity of 1200 mm/min was utilized. Lipids were detected in positive ion mode on a Bruker Daltonics 7T Solarix XR FTICR mass spectrometer system (Bruker Daltonics, Bremen, Germany) equipped with a dual ESI-MALDI (electrospray ionization matrix assisted laser desorption ionization) source employing Smartbeam-II technology. All images were collected in broadband mode covering m/z 150 −3000 utilizing 1500 shots per pixel and 120 μm pixel resolution. FTICR parameters were optimized to collect data at a resolution of ~150,000 for the lipid mass range of m/z 500–900, resulting in a 1 MW time-domain (0.7340 ms transient acquisition). Instrument settings were verified and performance qualified before each subsequent tissue analysis to ensure consistent data quality for the entire batch of tissue sections collected across multiple days. Imaging runs were acquired using FTMS control ver. 2.1, which generates real-time peak lists, or "sq. lite" files, that are directly compatible with SCiLS Lab (see 3D Volume Reconstruction). The apex method for online peak picking was selected with the maximum number of peaks set to 2500. The absolute minimum intensity for peak picking was set to 1.0 E5, with a signal to noise value of 4 (note: these parameters can be adjusted to include/exclude more data, per study design needs). Images were visualized in FlexImaging ver. 4.1 and normalized using RMS or root mean square.

Histological Staining

Following MALDI IMS acquisition, matrix was rinsed off the tissue using 100% methanol (~30 s). Rinsed tissues were stained with hematoxylin and eosin (H&E), as previously described [34], and optical images were collected on a Nanozoomer 2.0-RS slide scanner (Hamamatsu Photonics K.K., Japan). The stained images were imported as *. jpeg into FlexImaging and co-registered to the original optical image.

3D Volume Reconstruction

For reconstruction of the mouse lung volume, SCiLS Lab ver. 2015a (SCiLS, Bremen, Germany) was utilized on a supercomputer equipped with 192 GB of RAM and 2 × 2.90 GHz dual processors. Each individual imaging run (*.mis file) was compiled in sequential order into a single SCiLS experiment (*.sl file) by defining voxels based on lateral pixel resolution and distance between analyzed slices (120-um × 120-um × 120-um). Once all the individual tissue images were compiled into a single experiment, the process of creating a tissue volume could begin by using the individual optical scans from each tissue section collected. An anchor and point were placed on each optical image denoting features in the tissue that were conserved across neighboring tissue sections, thus serving as a fiduciary system. This anchor and point process was repeated for each pair of neighboring tissue sections until all sections were co-registered and a tissue volume rendered. The MS data were normalized using root mean square (RMS) and weakly de-noised. Visualization of the 3D reconstruction was performed in two modes, either slices or volumes.

Results and Discussion

The 3D workflow utilized in this proof of concept study was similar to conventional 2D IMS workflows; however, it differed in that the entire mouse lung was sectioned, with tissues collected for analysis every 120 μm (Figure 1). This process produced roughly 40 tissue sections numbered sequentially from the ventral to the dorsal sides of the lung, each of which were individually coated with matrix and analyzed via MALDI

IMS on a FTICR MS. Total analysis time was fairly rapid with an average run time of 2 h per tissue and an overall acquisition period of 2 weeks. In general, each individual tissue image produced roughly 60 GB (gigabyte) of raw data, for a total of over 2 TB (terabyte) of data representing all 40 sections. This prodigious amount of data could not be manipulated even with the most advanced super computers commercially available to date. However, with the opportunity to employ on-the-fly data reduction by generating peak lists, each individual image was decreased to around 3 GB, for a total of 150 GB, effectively reducing the original 2 TB dataset representing all 40 sections by >90%. Following data acquisition, each individual image file was compiled into a single experiment file in order to create the 3D volume. This process required each reduced image file to be loaded into the SCiLS Lab program, which took approximately 1–2 h per image, for a total of 50 h for the volume described here. Once all of the files were loaded, the sections were ordered based on chronological orientation and co-registered to one another for 3D reconstruction. The linear co-registration process involved defining features that were conserved across neighboring tissue sections, which would then serve as fiducials for the alignment of the two datasets. Once co-registration was achieved across the entire dataset, the lung volume could be rendered and manipulated. Additionally, although the entire lung volume was analyzed and reconstructed, for ease of visualization, the 3D volume shown here represents lung sections 12–28, with 12 being ventral and 28 dorsal.

As with conventional 2D MALDI IMS analyses, sample preparation and mode of acquisition can influence the types of analyte species detected. In the experiments described here, traditional lipid preparation and acquisition were employed,
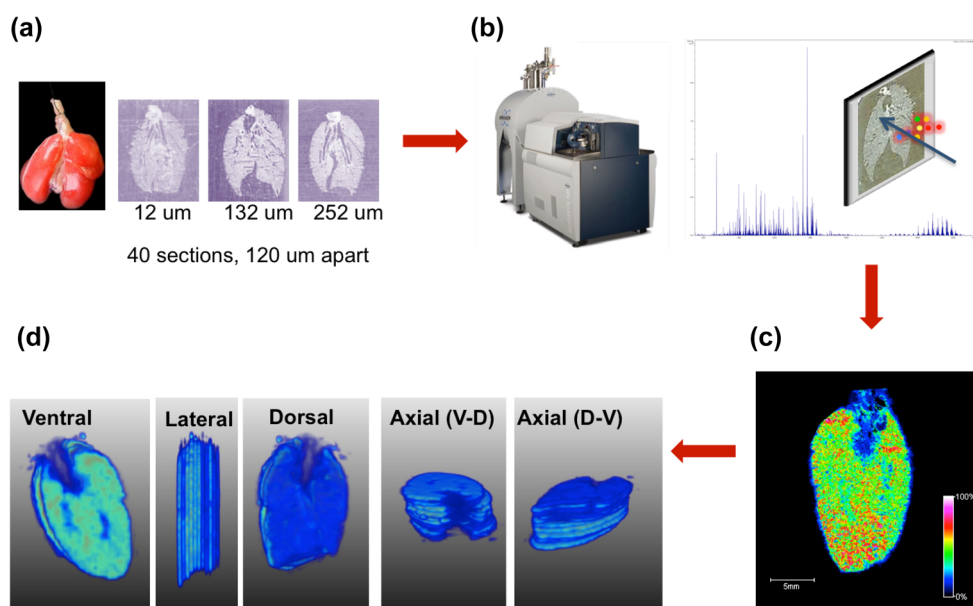

Figure 1. 3D MALDI FTICR IMS workflow. **(A)** For 3D reconstruction, a fresh frozen mouse lung was sectioned at 12 um, collecting tissues every 120 um for a total of 40 sections. Tissues were thaw mounted onto ITO coated slides and prepared for MALDI analysis. **(B)** Each slide was imaged on a MALDI FTICR MS. **(C)** Each individual tissue section was processed and 2D images visualized. **(D)** All tissue image datasets were compiled and co-registered to neighboring sections for 3D reconstruction. Once tissue volume is rendered, visualization can be performed from any vantage point

successfully producing images of various lipid species, including phosphatidylcholines (PC) and sphingomyelins (SM) (Supplementary Figures S1–S5). These lipid species are known to play important roles in lung biology, both as structural components for preventing alveolar collapse, and as mediators of inflammation and antiviral protection [4]. Across the 3D lung volume, lipid species with distinct distributions were detected, including species with ubiquitous detection throughout lung, while other species were only detected in the ventral versus dorsal regions of the lung. Figure 2 highlights examples of two ubiquitously distributed lipids across a cross-section of lung tissue, PC (16:0) $[M + Na]^+$ and PC (32:0) $[M + K]^+$. The individual 2D images all demonstrate a homogeneous detection of the lipid species across the tissue; however, when visualizing these lipids within the 3D volume, it becomes apparent that the relative abundance can vary based on location across the organ. For example, PC (16:0) $[M + Na]^+$ has uniform signal intensity across the entire lung volume regardless of vantage point, whereas PC (32:0) $[M + K]^+$ has a higher signal in the ventral versus the dorsal regions of the lung. It is unclear as to what the biological basis is for this observation. Extraction of the additional salt adducts of this lipid verified the distribution across the lung volume (data not shown), and suggested that the observed distributions were not reflective of differential adduct formation or bias introduced during the course of the tissue preparations and image acquisitions. Further, this differential expression does not appear to be unique to PC lipids and is also seen in 3D images of several SM lipids. For example, SM (d40:1) $[M + Na]^+$ is observed to have higher signal in the ventral versus dorsal regions of the lung volume (Figure 3). Although an experimentally induced artifact cannot be

SM (d40:1) [M+Na]⁺ m/z 809.580

Figure 3. Differential localization of SM in the lung tissue. **(A)** SM (d40:1) $[M + Na]^+$ m/z 809.580 2D distribution in ventral and dorsal sections. **(B)** 3D volume of SM (d40:1) $[M + Na]^+$ m/z 809.580 from both ventral and dorsal vantage

definitively excluded, it is believed to be unlikely, since numerous lipid signals were observed to have consistent
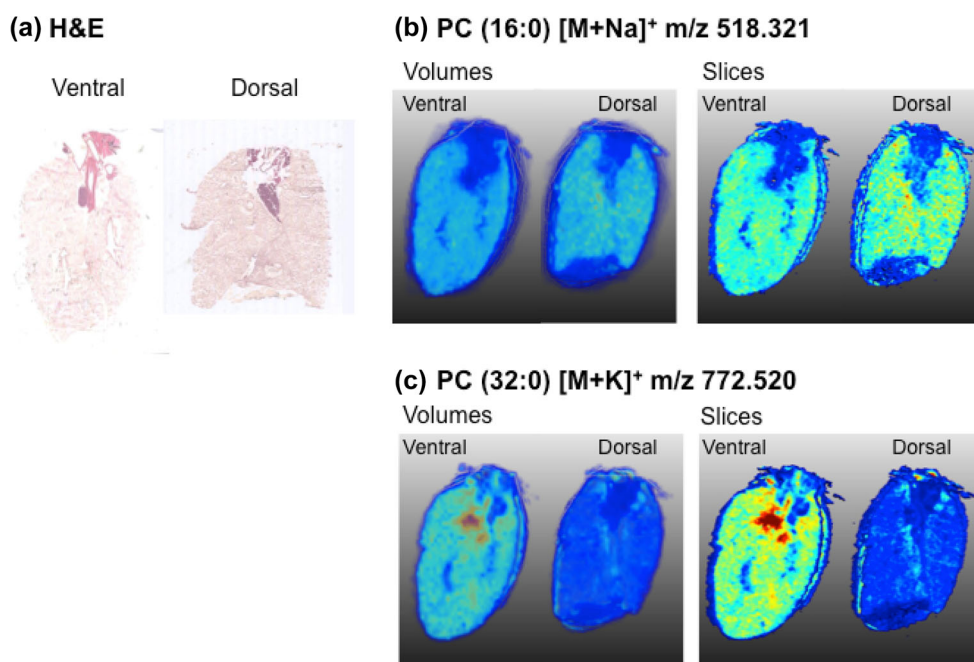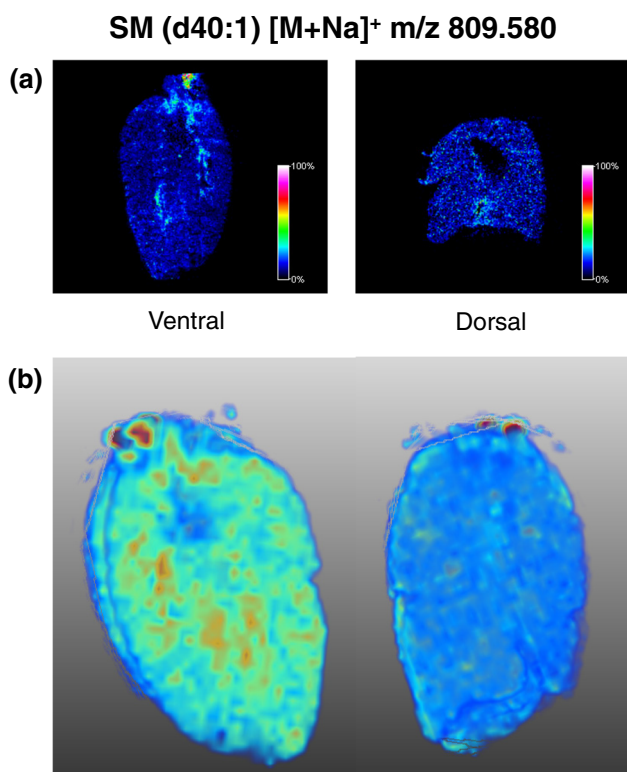

Figure 2. MALDI FTICR IMS 3D volumes can allow for nimble assessments of analyte distribution across an entire organ. **(A)** An H&E stain of ventral and dorsal sections of the mouse lung. **(B)** PC (16:0) $[M + Na]^+$. **(C)** PC (32:0) $[M + K]^+$ 3D distributions in the mouse lung shown as volume or slices view, from both the ventral and dorsal vantage
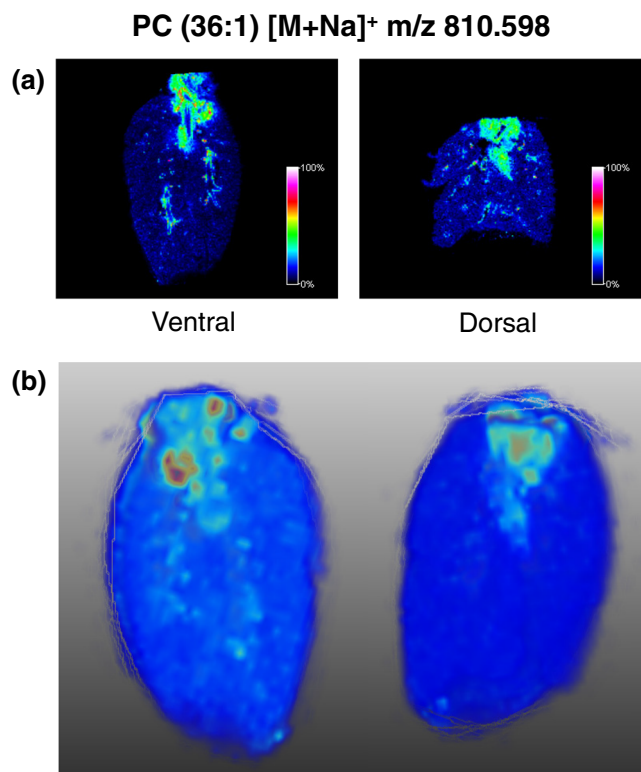
PC (36:1) [M+Na]⁺ m/z 810.598

Figure 4. Substructure localization of PC in the major bronchus. **(A)** PC (36:1) [M + Na]⁺ *m/z* 810.598 2D distribution in ventral and dorsal sections. **(B)** 3D volume of PC (36:1) [M + Na]⁺ *m/z* 810.598 from both ventral and dorsal vantage

intensities across the entire lung volume, such as the aforementioned PC (16:0) [M + Na]⁺. Additionally, a consistent internal standard response was achieved for each section in the volume, which served as an added level of quality control. Nevertheless,

this observation serves to demonstrate the advantage of a 3D MALDI IMS approach, as it allows for nimble assessments of not only cross-sectional (2D), but also global (3D) distributions of analyte signals across an entire organ.

Combining the MALDI IMS analysis with histological staining adds another dimension to aid in the interpretation of analyte distribution studies. For the mouse lung described here, a number of lipid species, such as PC (36:1) [M + Na]⁺ and SM (d34:1) [M + K]⁺, were observed to have localization to specific substructures (Figures 4 and 5, respectively). Identification of the exact anatomical features from a single H&E lung section can be quite difficult. For example, similar morphologic arrangements of stromal and epithelial cells are observed for the closely oriented esophagus and major bronchus, which can allow for these substructures to be easily misidentified (Supplementary Figure S6). However, when observing these histologic stains in the context of a 3D volume, positive identification of substructure assignments can be easily confirmed and confidently related back to the lipid distribution. In the case of PC (36:1) [M + Na]⁺, its localization can be attributed to the major bronchus, whereas localization of SM (d34:1) [M + K]⁺ corresponds to the esophagus. In theory, one could section the entire lung and analyze representative sections throughout the volume to obtain a similar confirmation of substructure localization. Moreover, the 3D reconstruction is advantageous since it allows for the visualization of analytes in the context of an entire organ, or in relation to other specific levels in the volume. Thus the reconstructed 3D image is dynamic, and analyte distributions can be viewed within any plane or perspective of interest, and is demonstrated with esophageal-specific SM (d34:1) [M + K]⁺ in Figure 6. Even more enthralling is the capacity to rotate the 3D image in 360° space, as well as record a movie of this rotation (Supplementary Movie S7).
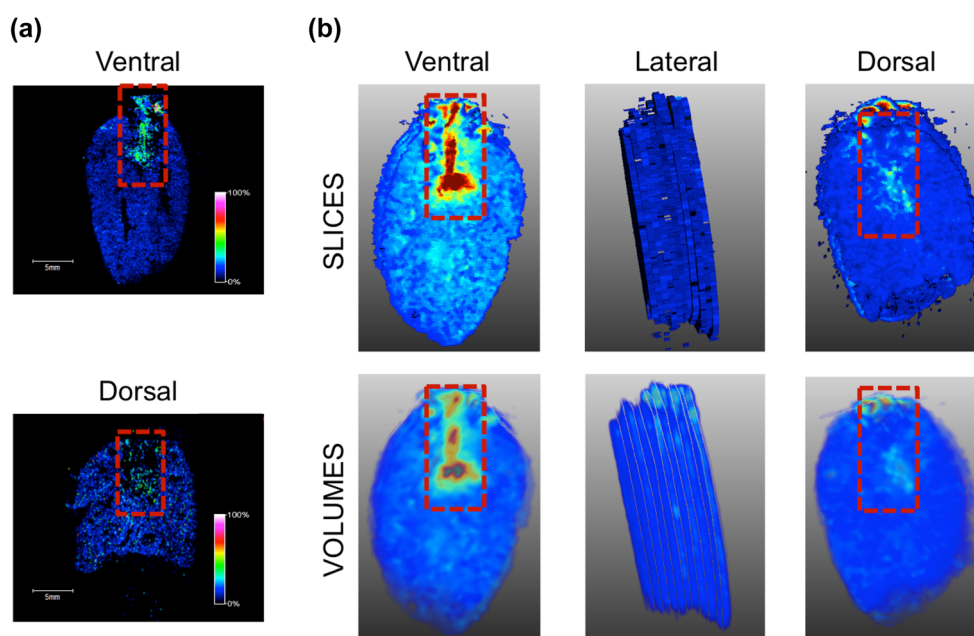

Figure 5. Substructure localization of SM in the esophagus. **(A)** 2D distribution of SM (d34:1) [M + K]⁺ *m/z* 741.526 in the ventral and dorsal view. **(B)** 3D volume of SM (d34:1) [M + K]⁺ *m/z* 741.526 from the ventral, lateral, and dorsal vantage points
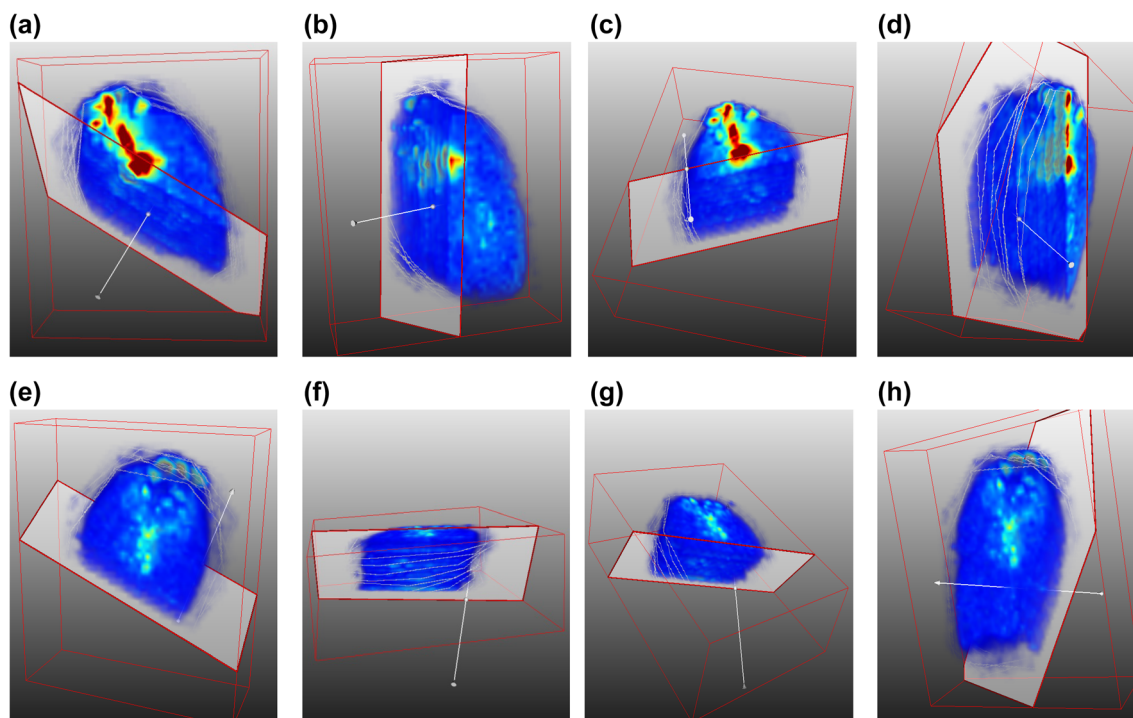
Figure 6. Distribution of SM from various perspectives originating from both ventral **(A)**–**(D)**, and dorsal **(E)**–**(H)** vantage points. 3D images of SM (d34:1) [M + K]$^+$ m/z 741.526

These examples highlight the advantages of a 3D imaging approach and the importance of interpreting 2D images within the context of the whole organ, where caution should be exercised when drawing conclusions from a single cross-section. Although the analytes highlighted here are endogenous lipids, in the pharmaceutical industry where high resolution MALDI IMS is often used to assess drug and metabolite localization in treatment models, only sectioning part of the lung could have significant implications. For example in the case of intranasal dosing studies, it is known that over 90% the drug is swallowed. Therefore, assessments of drug distribution via an intranasal dose may appear to indicate drug localization in the major bronchus when, in fact, drug is present in the esophagus due to swallowing. As this initial study only served to demonstrate the feasibility of producing 3D images from a MALDI FTICR dataset, it will be interesting to observe the impact of future 3D MALDI FTICR IMS studies and their ability to assess relevant biological and pharmacological questions in relation to disease or dose response.

Conclusions

MALDI FTICR IMS datasets can be successfully used to produce 3D volumes when proper conditions are collectively considered, including data reduction, visualization software, and a super-computer for processing. Advantages of 3D MALDI FTICR IMS datasets include a more thorough representation of thousands of analyte distributions across an entire organ. Representative lipids detected in mouse lung

demonstrated the ability to differentiate analyte distributions across the tissue cross-section, as well as, in the context of the entire organ. More confident assessments regarding substructure localizations could also be made with the 3D approach.

Although innovative and exciting, there are still many aspects of 3D volume reconstruction using FTICR data sets that will need to be considered. Although the current software advancements have successfully allowed for real-time data reduction into peak lists, overall successful compilation of serial images remains limited to smaller datasets. Conceivably, selecting more stringent reduction parameters, or collecting lower pixel resolution images, could aid in circumventing these current limitations, but should be balanced with the goals and needs of the 3D experiment. Nevertheless, it would be prudent that each imaging facility wishing to perform this type of workflow have super computers and adequate data storage plans in place. Additionally, further attention should be placed on identifying a robust co-registration procedure that is independent of tissue features (e.g., external fiduciary system) or employ non-linear co-registration methods. With the current linear co-registration approach, differences in location of common features between adjacent sections could be compromised during the sectioning and tissue mounting steps, and will influence the accuracy to which neighboring sections will be co-registered. Moreover, as the tissue sections are collected through different levels of a whole organ such as lung, teachings based on common features can vary in size and will contribute to stretching and misalignment of the final rendering, producing undesirable edge effects and distorted volumes. Admittedly, this was a very limited demonstration of a 3D

MALDI FTICR IMS approach, and despite these recognized challenges, the study described here highlights the potential advantages of a 3D experiment. As the mass spectrometry imaging field moves into novel areas, such as in situ metabolomics, the possibility of including FT data for 3D reconstruction is exciting, especially where clear advantages of a high mass resolution imaging approach are already well understood.

Acknowledgements

References

1. Aichler, M., Walch, A.: MALDI imaging mass spectrometry: current frontiers and perspectives in pathology research and practice. Lab. Invest. **95**, 422–431 (2015)

2. Gessel, M.M., Norris, J.L., Caprioli, R.M.: MALDI imaging mass spectrometry: spatial molecular analysis to enable a new age of discovery. J. Proteome. **107**, 71–82 (2014)

3. Spraggins, J.M., Rizzo, D.G., Moore, J.L., Rose, K.L., Hammer, N.D., Skaar, E.P.: MALDI FTICR IMS of Intact Proteins: Using Mass Accuracy to Link Protein Images with Proteomics Data. J. Am. Soc. Mass Spectrom. **26**, 974–985 (2015)

4. Berry, K.A., Li, B., Reynolds, S.D., Barkley, R.M., Gijon, M.A., Hankin, J.A.: MALDI imaging MS of phospholipids in the mouse lung. J. Lipid Res. **52**, 1551–1560 (2011)

5. Gessel, M., Spraggins, J.M., Voziyan, P., Hudson, B.G., Caprioli, R.M.: Decellularization of intact tissue enables MALDI imaging mass spectrometry analysis of the extracellular matrix. J. Mass Spectrom. **50**, 1288–1293 (2015)

6. Groseclose, M.R., Laffan, S.B., Frazier, K.S., Hughes-Earle, A., Castellino, S.: Imaging MS in toxicology: an investigation of juvenile rat nephrotoxicity associated with dabrafenib administration. J. Am. Soc. Mass Spectrom. **26**, 887–898 (2015)

7. Jones, E.E., Dworski, S., Canals, D., Casas, J., Fabrias, G., Schoenling, D.: On-tissue localization of ceramides and other sphingolipids by MALDI mass spectrometry imaging. Anal. Chem. **86**, 8303–8311 (2014)

8. Powers, T.W., Jones, E.E., Betesh, L.R., Romano, P.R., Gao, P., Copland, J.A.: Matrix assisted laser desorption ionization imaging mass spectrometry workflow for spatial profiling analysis of N-linked glycan expression in tissues. Anal. Chem. **85**, 9799–9806 (2013)

9. Quiason, C.M., Shahidi-Latham, S.K.: Imaging MALDI MS of dosed brain tissues utilizing an alternative analyte pre-extraction approach. J. Am. Soc. Mass Spectrom. **26**, 967–973 (2015)

10. Yalcin, E.B., de la Monte, S.M.: Review of matrix-assisted laser desorption ionization-imaging mass spectrometry for lipid biochemical histopathology. J. Histochem. Cytochem. **63**, 762–771 (2015)

11. Dufresne, M., Masson, J.F., Chaurand, P.: Sodium-doped gold-assisted laser desorption ionization for enhanced imaging mass spectrometry of triacylglycerols from thin tissue sections. Anal. Chem. **88**, 6018–6025 (2016)

12. Friesen, W.L., Schultz, B.J., Destino, J.F., Alivio, T.E., Steet, J.R., Banerjee, S.: Two-dimensional graphene as a matrix for MALDI imaging mass spectrometry. J. Am. Soc. Mass Spectrom. **26**, 1963–1966 (2015)

13. Lagarrigue, M., Caprioli, R.M., Pineau, C.: Potential of MALDI imaging for the toxicological evaluation of environmental pollutants. J Proteome. **144**, 133–139 (2016)

14. Niehoff, A.C., Kettling, H., Pirkl, A., Chiang, Y.N., Dreisewerd, K., Yew, J.Y.: Analysis of Drosophila lipids by matrix-assisted laser desorption/ionization mass spectrometric imaging. Anal. Chem. **86**, 11086–11092 (2014)

15. Wakeman, C.A., Moore, J.L., Noto, M.J., Zhang, Y., Singleton, M.D., Prentice, B.M.: The innate immune protein calprotectin promotes *Pseudomonas aeruginosa* and *Staphylococcus aureus* interaction. Nat. Commun. **7**, 11951 (2016)

16. Ly, A., Buck, A., Balluff, B., Sun, N., Gorzolka, K., Feuchtinger, A.: High-mass-resolution MALDI mass spectrometry imaging of metabolites from formalin-fixed paraffin-embedded tissue. Nat. Protoc. **11**, 1428–1443 (2016)

17. Shahidi-Latham, S.K., Dutta, S.M., Prieto Conaway, M.C., Rudewicz, P.J.: Evaluation of an accurate mass approach for the simultaneous detection of drug and metabolite distributions via whole-body mass spectrometric imaging. Anal. Chem. **84**, 7158–7165 (2012)

18. Thiele, H., Heldmann, S., Trede, D., Strehlow, J., Wirtz, S., Dreher, W.: 2D and 3D MALDI imaging: conceptual strategies for visualization and data mining. Biochim. Biophys. Acta **1844**, 117–137 (2014)

19. Aswendt, M., Schwarz, M., Abdelmoula, W.M., Dijkstra, J., Dedeurwaerdere, S.: Whole-brain microscopy meets in vivo neuroimaging: techniques, benefits, and limitations. Mol. Imaging Biol. **19**, 1–9 (2017)

20. Cuccurullo, V., Di Stasio, G.D., Schilliro, M.L., Mansi, L.: Small-animal molecular imaging for preclinical cancer research:.μPET and μ.SPECT. Curr. Radiopharm. **9**, 102–113 (2016)

21. Sridhar, S., Mishra, S., Gulyas, M., Padmanabhan, P., Gulyas, B.: An overview of multimodal neuroimaging using nanoprobes. Int. J. Mol. Sci. **18** (2017)

22. Ferreira, C.A., Fuscaldi, L.L., Townsend, D.M., Rubello, D., Barros, A.L.: Radiolabeled bombesin derivatives for preclinical oncological imaging. Biomed. Pharmacother. **87**, 58–72 (2017)

23. Crecelius, A.C., Cornett, D.S., Caprioli, R.M., Williams, B., Dawant, B.M., Bodenheimer, B.: Three-dimensional visualization of protein expression in mouse brain structures using imaging mass spectrometry. J. Am. Soc. Mass Spectrom. **16**, 1093–1099 (2005)

24. Seeley, E.H., Caprioli, R.M.: 3D imaging by mass spectrometry: a new frontier. Anal. Chem. **84**, 2105–2110 (2012)

25. Andersson, M., Groseclose, M.R., Deutch, A.Y., Caprioli, R.M.: Imaging mass spectrometry of proteins and peptides: 3D volume reconstruction. Nat. Methods **5**, 101–108 (2008)

26. Patterson, N.H., Doonan, R.J., Daskalopoulou, S.S., Dufresne, M., Lenglet, S., Montecucco, F.: Three-dimensional imaging MS of lipids in atherosclerotic plaques: open-source methods for reconstruction and analysis. Proteomics **16**, 1642–1651 (2016)

27. Trede, D., Schiffler, S., Becker, M., Wirtz, S., Steinhorst, K., Strehlow, J.: Exploring three-dimensional matrix-assisted laser desorption/ionization imaging mass spectrometry data: three-dimensional spatial segmentation of mouse kidney. Anal. Chem. **84**, 6079–6087 (2012)

28. Liu, X., Hummon, A.B.: Mass spectrometry imaging of therapeutics from animal models to three-dimensional cell cultures. Anal. Chem. **87**, 9508–9519 (2015)

29. Oetjen, J., Veselkov, K., Watrous, J., McKenzie, J.S., Becker, M., Hauberg-Lotte, L.: Benchmark datasets for 3D MALDI- and DESI-imaging mass spectrometry. Gigascience **4**, 20 (2015)

30. Palmer, A.D., Alexandrov, T.: Serial 3D imaging mass spectrometry at its tipping point. Anal. Chem. **87**, 4055–4062 (2015)

31. Trede, D., Kobarg, J.H., Oetjen, J., Thiele, H., Maass, P., Alexandrov, T.: On the importance of mathematical methods for analysis of MALDI-imaging mass spectrometry data. J. Integr. Bioinform. **9**, 189 (2012)

32. Sinha, T.K., Khatib-Shahidi, S., Yankeelov, T.E., Mapara, K., Ehtesham, M., Cornett, D.S.: Integrating spatially resolved three-dimensional MALDI IMS with in vivo magnetic resonance imaging. Nat. Methods **5**, 57–59 (2008)

33. Marshall, A.G., Hendrickson, C.L., Jackson, G.S.: Fourier transform ion cyclotron resonance mass spectrometry: a primer. Mass Spectrom. Rev. **17**, 1–35 (1998)

34. Chaurand, P., Schwartz, S.A., Billheimer, D., Xu, B.J., Crecelius, A., Caprioli, R.M.: Integrating histology and imaging mass spectrometry. Anal. Chem. **76**, 1145–1155 (2004)